EFFECT OF NEUTRON SOURCE ON THE INCINERATION OF LIGHT WATER REACTORS WASTE BY PRISMATIC HIGH TEMPERATURE REACTORS

Jitka Zakova[1] and Alberto Talamo[2]

[1]*Royal Institute of Technology (KTH), Roslagstullsbacken 21, S-10691 Stockholm, Sweden*
Email: jitka@neutron.kth.se
[2]*Argonne National Laboratory (ANL), 9700 S. Cass Ave., Argonne, 60439 IL, USA*

The present study investigates the effect of neutron source on the incineration of Light Water Reactors waste by the Gas Turbine – Modular Helium Reactor. Three different core configurations have been analyzed: critical, accelerator and fusion driven systems. In the accelerator driven system, neutrons are generated by a 1000 MeV proton beam interacting with a lead target. In the fusion driven system, neutrons are generated, in the center of the core, with a fixed energy of 14.1 MeV, through a deuterium-tritium reaction. The comparison of the actinides transmutation for the three configurations shows unclear benefits for the driven systems.

I. INTRODUCTION

The incineration of nuclear waste by a subcritical Gas Turbine – Modular Helium Reactor (GT-MHR) [1-4] was originally proposed by Baxter et al. [5]; then, it was investigated by Rodriguez et al. [6], Gohar et al. [7-8] and Ridikas et al. [9]. The present study contributes to the previous investigations and it focuses on the actinides transmutation in three different configurations of the GT-MHR: 1) critical core, 2) accelerator driven system and 3) fusion driven system. The major differences between the three configurations are the neutron source spectrum and location. In the critical core, neutrons are generated, with an average energy of 2 MeV, in the TRISO fuel particles. In the accelerator driven system, neutrons are generated in the center of the core through a spallation reaction induced by a 1000 MeV proton beam. In the fusion driven system, neutrons are generated, with a fixed energy of 14.1 MeV, in the center of the core through a deuterium-tritium (DT) reaction. There are two major benefits of a driven system: first, a subcritical system offers a higher degree of security in the nuclear power plant; second, the spectrum of the neutron source favors actinides fissioning. In the thermal energy range (where the GT-MHR operates), the fission to capture ratio of non-fissile plutonium and minor actinides isotopes, from Light Water Reactors (LWRs) waste, is small or negligible. Consequently, in order to improve the fission to capture ratio of non-fissile fuel actinides General Atomics advertised the subcritical GT-MHR [6] putting emphasis on the faster spectrum set by the spallation/DT reaction.

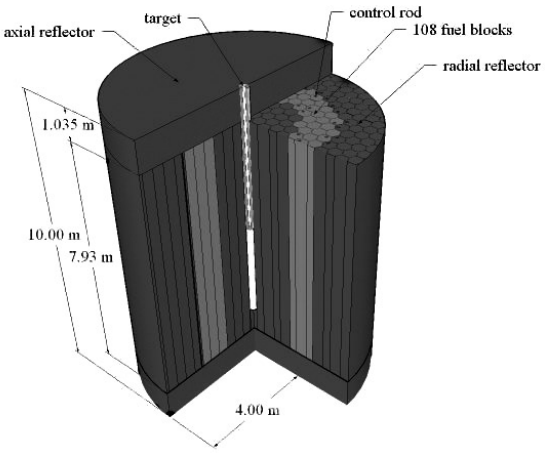

Figure 1: Accelerator Driven GT-MHR.

II. METHODOLOGY OF CALCULATION

A detailed modeling of the GT-MHR has been implemented without any fuel homogenization by the MCNP code [10]. The model includes the description of burnable poison and control rods [11-12]. Tables I and II report the geometry and the material data of the present core, respectively.

Table I: Core design parameters

Core	
Radius [cm]	400
Active height [cm]	793
Axial pure graphite reflectors height top/bottom [cm]	103.5
Number of fuel blocks in the core	108
Power [MW_{th}]	600
Hexagonal Fuel Blocks	
Apothem [cm]	18
Height [cm]	793
Number of fuel pins in the block	216
Radius of the fuel channels [cm]	0.635
Number of coolant channels in the block	108
Radius of the coolant channel [cm]	0.795
Fuel Pins	
Radius [cm]	0.622
Height [cm]	793
Packing fraction (TRISO volume over pin volume)	10%
Graphite density [$g \cdot cm^{-3}$]	1.74
TRISO Particles	
Kernel radius [μm]/density [$g \cdot cm^{-3}$]	150/10.36
Porous carbon outer radius [μm]/density [$g \cdot cm^{-3}$]	300/1.0
Pyrocarbon outer radius [μm]/density [$g \cdot cm^{-3}$]	335/1.85
Zirconium carbide outer radius [μm]/density [$g \cdot cm^{-3}$]	370/6.56
Pyrocarbon outer radius [μm]/density [$g \cdot cm^{-3}$]	410/1.85
Burnable Poison Particles	
Kernel radius [μm]/density [$g \cdot cm^{-3}$] - fission	130/7.28
Kernel radius [μm]/density [$g \cdot cm^{-3}$] - ADS	160/7.28
Kernel radius [μm]/density [$g \cdot cm^{-3}$] - fusion	160/7.28
Porous carbon outer radius [μm]/density [$g \cdot cm^{-3}$]	175/1.0
Pyrocarbon outer radius [μm]/density [$g \cdot cm^{-3}$]	210/1.85
Target	
Beam energy [MeV]	1000
Beam radius [cm]	2
Beam tube radius [cm]	5
Beam tube cladding outer radius [cm]	5.5
Target inner radius [cm]	14.5
Target cladding outer radius [cm]	15
Fusion	
Neutron energy [MeV]	14.1
Source radius [cm]	15
Source height [cm]	15

Table II: Fuel atomic composition

Isotope	Percentage [%]
^{237}Np	1.83
^{238}Pu	0.63
^{239}Pu	20.23
^{240}Pu	8.4
^{241}Pu	1.99
^{242}Pu	1.36
^{241}Am	2.10
^{243}Am	0.33
^{242}Cm	0.04
^{244}Cm	0.11
^{16}O	62.96

All burnup calculations have been performed by the MCB code [13-15], which is the only Monte Carlo code with the capability to simulate the burnup of a subcritical system. In the case of the accelerator driven system, the spallation reaction has been simulated by the MCNPX code [16] and the resulting MCNPX neutron source has been passed to the MCB code. Figure 1 illustrates the accelerator driven GT-MHR; figure 2 shows the spallation target details.

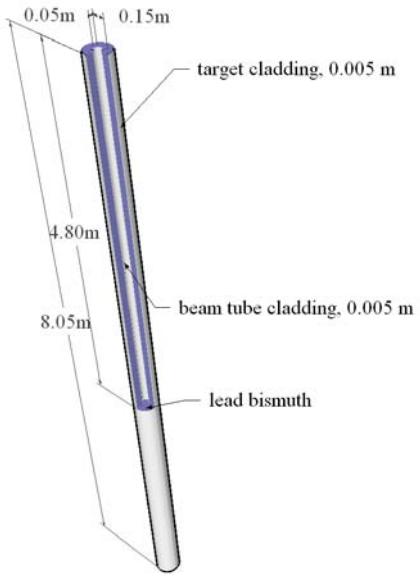

Figure 2: Spallation target.

III. NEUTRON SPECTRUM

Figure 3 illustrates the neutron spectrum resulting from a spallation reaction generated by a 1000 MeV proton beam interacting with a lead target. The spectrum hardens when the radius diminishes down to 10-15 cm; consequently, a value of 15 cm has been used for the rest of the present study. The neutron spectrum coming from a spallation reaction exhibits a peak at 1 MeV and a tail that extends to several hundreds MeV (that is the part of the spectrum expected to augment the fission to capture ratio of non-fissile actinides).

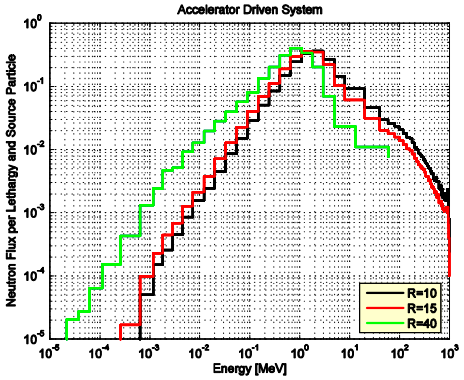

Figure 3: Neutron spectrum (normalized to 1) of a spallation reaction with a lead target.

Figure 4 shows the neutron spectrum averaged in the TRISO fuel kernels, in the graphite hexagonal blocks next to the target (first ring), and in the graphite hexagonal blocks next to the inner fuel ring (fourth ring) for the accelerator driven GT-MHR. In the graphite hexagonal blocks, the spectrum is well thermalized; however, the fast tail of the spectrum is higher in the blocks that are closer to the target (first ring). The spectrum in the TRISO fuel kernels exhibits a faster profile and it shows two distinct dips at 0.3 and 1 eV; the latter ones are generated by ^{239}Pu and ^{240}Pu resonances, respectively. Figures 5 and 6 repeat the plot of figure 4 for the fusion driven and critical GT-MHR, respectively; the remarks, previously stated for the accelerator driven GT-MHR, hold.

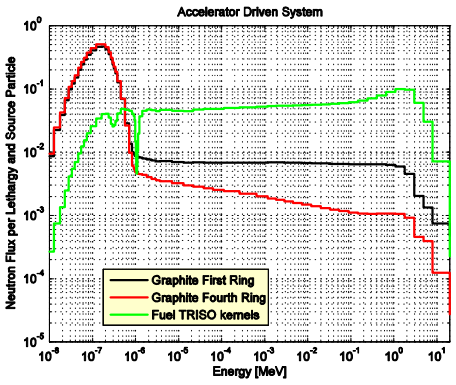

Figure 4: Neutron spectrum (normalized to 1) averaged in the graphite blocks next to the target (first ring), in the graphite blocks next to the inner fuel ring (fourth ring), and in the TRISO fuel kernels. Accelerator driven GT-MHR.

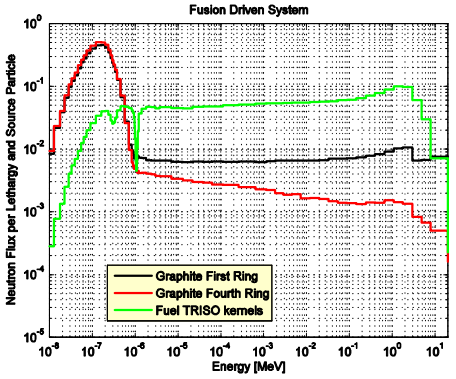

Figure 5: Neutron spectrum (normalized to 1) averaged in the graphite blocks next to the target (first ring), in the graphite blocks next to the inner fuel ring (fourth ring), and in the TRISO fuel kernels. Fusion driven GT-MHR.

As expected, in the critical GT-MHR, the fast tail of the spectrum, averaged in the graphite hexagonal blocks, is higher when the blocks are next to the fuel (fourth ring). The comparison of figures 4, 5 and 6 reveals that the spectrum averaged in the TRISO fuel kernels is little influenced by the external source.

IV. EXCESS OF REACTIVITY

Figure 7 shows, for the three core configurations, the multiplication factors k_{eff} and k_{src} as function of time.

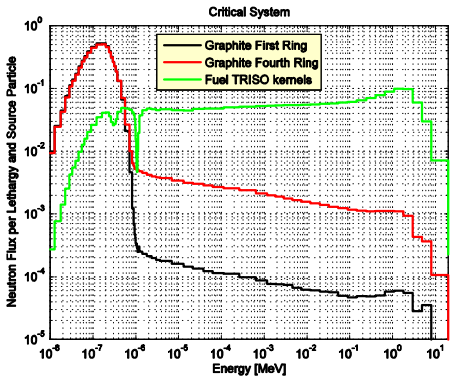

Figure 6: Neutron spectrum (normalized to 1) averaged in the graphite blocks next to the target (first ring), graphite blocks next to the inner fuel ring (fourth ring), and in the TRISO fuel kernels. Critical GT-MHR.

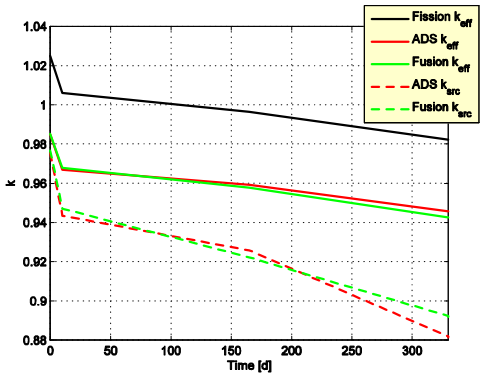

Figure 7: k_{eff} as function of time during 330 irradiation days. Accelerator and fusion driven systems and critical core.

During burnup, the control rods were always fully inserted. The subcritical status of the driven systems has been set by increasing the radius of the BISO burnable poison (Eu_2O_3) kernels from 130 μm up to 160 μm. After 330 irradiation days, the initial excess/defect of reactivity diminishes of 4000 pcm. In the present core configuration, k_{src} is smaller than k_{eff} and the difference amplifies during irradiation. The previous effect is due to the displacement of the external neutron source in a position where the neutron flux in the core is depressed; that sets a bad neutron economy. In an optimal design of a subcritical system, k_{src} is larger than k_{eff}; that invites to further studies about alternative configurations for the subcritical GT-MHR.

Table III lists the k_{eff} values at the beginning and end of irradiation for the three core configurations. At the beginning of irradiation, the operational control rods worth is about 7000 pcm; after 330 irradiation days, it increases up to 9400-11000 pcm.

Table III: k_{eff} values at the beginning and end of irradiation with and without control rods.

	k_{eff} with inserted control rods	
	0 days	**330 days**
Fission	1.024850 ± 0.00027	0.955549 ± 0.00024
ADS	0.984960 ± 0.00031	0.931102 ± 0.00033
Fusion	0.985136 ± 0.00031	0.925657 ± 0.00029
	k_{eff} with withdrawn control rods	
	0 days	**330 days**
Fission	1.09406 ± 0.00025	1.06561 ± 0.00028
ADS	1.05234 ± 0.00028	1.02502 ± 0.00027
Fusion	1.05267 + 0.00027	1.02439 ± 0.00028

V. ACTINIDES TRANSMUTATION

Figures 8 and 9 plot the actinides mass at the beginning and end of irradiation for the three GT-MHR configurations. At first glance, it appears that the benefit of using a subcritical GT-MHR is not clear, since there is a negligible difference between the critical and subcritical core in the transmuted actinide masses (as expected form the neutron spectrum analyses). The major drawback of the incineration of LWRs waste by the GT-MHR is the accumulation of minor actinides [2-4]; that is not solved with the present subcritical configurations.

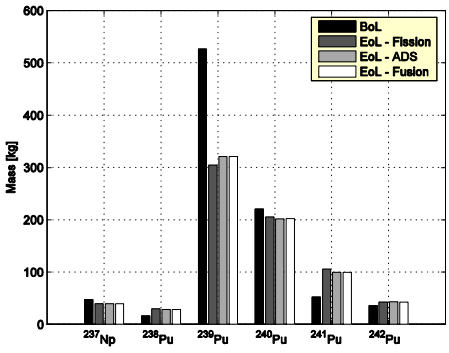

Figure 8: Neptunium and plutonium mass as function of time. Accelerator and fusion driven systems and critical core.

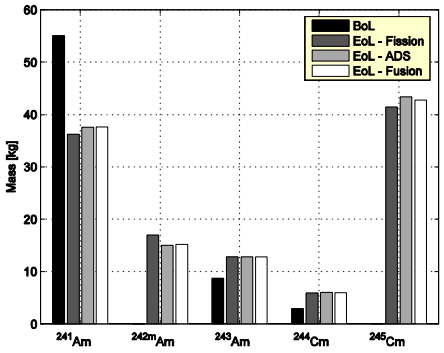

Figure 9: Americium and curium mass as function of time. Accelerator and fusion driven systems and critical core. The mass of ^{242m}Am and ^{245}Cm have been multiplied by 10 and 100, respectively.

VI. CONCLUSIONS

The subcritical configurations of the GT-MHR proposed by General Atomics have shown unclear benefits. In fact, the transmuted actinide masses are similar to those obtained by a critical core; that is caused by the small influence of the external neutron source to the neutron spectrum averaged in the TRISO kernels. The present design has shown that k_{eff} is larger than k_{src}; that indicates a quite bad neutron economy.

ACKNOWLEDGMENTS

Special thanks to Dr. Kamil Tucek (JRC, Petten, Netherlands) for the help in designing the target, to Deputy Executive Director and Chair Professor Waclaw Gudowski (ISTC, Moskow, Russia) for processing nuclear data libraries and to Professor Jerzy Cetnar (AGH, Cracow, Poland) for the help in linking MCNPX to MCB.

REFERENCES

[1] GENERAL ATOMICS, *GT-MHR conceptual design description report*, GA/NRC-337-02, (2002).

[2] A. TALAMO et al., "The Burnup Capabilities of the Deep Burn Modular Helium Reactor Analyzed by the Monte Carlo Continuous Energy Code MCB," *Annals of Nuclear Energy* **31/2**, pp. 173-196, (2004).

[3] A. TALAMO et al., "Comparison of MCB and MONTEBURNS Monte Carlo Burnup Codes on a One-Pass Deep Burn," *Annals of Nuclear Energy* **33/14-15**, pp. 1176-1188, (2006).

[4] A. TALAMO and W. GUDOWSKI, "Incineration of Light Water Reactors waste in High Temperature Gas Reactors: Axial Fuel Management and Strategy for Transmutation of Americium and Curium," *Nuclear Science and Engineering* **156**, (2007).

[5] A. BAXTER et al., *The Two-Level Helium Cycle for Maximum Transmutation in Secure, Clean and Safe Manner*, Los Alamos National Laboratory, LA-UR-00-5616, (2000).

[6] C. RODRIGUEAZ et al., "Deep Burn: Making Nuclear Waste Transmutation Practical," *Nuclear Engineering and Design* **222/2-3**, (2003).

[7] Y. GOHAR et al., *Assessment of the General Atomics Accelerator Transmutation of Waste Concept Based on the Gas-Turbine-Modular Helium Cooled Reactor Technology*, Argonne National Laboratory, ANL/TD/TM01/16, (2001).

[8] Y. GOHAR et al., *Neutronics Verification of General Atomics Accelerator Transmutation of Waste Concept*, Argonne National Laboratory, ANL/TD/TM01/17, (2001).

[9] D. RIDIKAS et al., "Critical and Subcritical GT-MHRs for Waste Disposal and Proliferation-Resistant Fuel Cycles," *Proceedings of the 6th OECD/NEA Information Exchange Meeting on Actinide and Fission Product Partitioning and Transmutation*, Madrid, Spain, 11-13 December, (2000).

[10] J.F. BRIESMEISTER, *A general Monte Carlo N-Particle transport code – version 4c*, Los Alamos National Laboratory, LA-13709-M, (2002).

[11] A. TALAMO, "Managing the Reactivity Excess of the Gas Turbine - Modular Helium Reactor by Burnable Poison and Control Rods," *Annals of Nuclear Energy* **33/1**, pp. 84-98, (2006).

[12] A. TALAMO, "Effects of the Burnable Poison Heterogeneity on the Long Term Control of Excess of Reactivity," *Annals of Nuclear Energy* **33/9**, pp. 794-803, (2006).

[13] J. CETNAR et al., *MCB: a continuous energy Monte Carlo burnup simulation code in actinide and fission product partitioning and transmutation*, EUR 18898 EN, OECD/NEA 523, (1999).

[14] J. CETNAR, "General solution of Bateman equations for nuclear transmutations," *Annals of Nuclear Energy* **33/7**, pp. 640-645, (2006).

[15] A. TALAMO et al., "MCB1c2 Bug on Thermal Reactors," *Annals of Nuclear Energy* **33/7,** pp. 653-654, (2006).

[16] J.S. HENDRICKS et al, *MCNPX, Version 2.6.b*, Los Alamos National Laboratory, LA-UR-06-3248, (2006).